

# Black-Body Stars

Nao Suzuki

*Kavli Institute for the Physics and Mathematics of the Universe, University of Tokyo,  
Kashiwa 277-8583 Japan*

Masataka Fukugita

*Kavli Institute for the Physics and Mathematics of the Universe, University of Tokyo,  
Kashiwa 277-8583 Japan*

*Institute for Advanced Study, Princeton NJ08540, U.S.A.*

## ABSTRACT

We report the discovery of stars that show spectra very close to the black-body radiation. We found 17 such stars out of 798,593 stars in the Sloan Digital Sky Survey (SDSS) spectroscopic data archives. We discuss the value of these stars for the calibration of photometry, whatever is the physical nature of these stars. This gives us a chance to examine the accuracy of the zero point of SDSS photometry across various passbands: we conclude that the zero point of SDSS photometric system is internally consistent across its five passbands to the level below 0.01 mag. We may also examine the consistency of the zero-points between UV photometry of Galaxy Evolution Explorer and SDSS, and IR photometry of Wide-field Infrared Survey Explorer against SDSS. These stars can be used as not only photometric but spectrophotometric standard stars. We suggest that these stars showing the featureless black-body like spectrum of the effective temperature of  $10000 \pm 1500\text{K}$  are consistent with DB white dwarfs with the temperature too low to develop helium absorption features.

## 1. Introduction

We report the discovery of stars that have nearly a perfect black-body spectrum without any features in the wavelength range from ultraviolet to infrared. A search is made for objects with featureless spectrum in the spectral archives of the Sloan Digital Sky Survey (SDSS)(Abazajian et al. 2009; Alam et al. 2015), supplemented with Galaxy Evolution Explorer (GALEX)(Morrissey et al. 2007) and Wide-field Infrared Survey Explorer (WISE)(Wright et al. 2010). We find 17 objects whose spectral energy distribution is consistent with a black-body radiation to a high accuracy in

the UV (GALEX; FUV, NUV), the optical (SDSS;  $u, g, r, i, z$ ,) and in the infrared (WISE; W1). These stars all are  $r > 17$ . The physical identity of these objects is yet to be confirmed, but we find that they are consistent with DB white dwarfs with a low temperature. Whatever is the nature of the objects, we emphasize a practical value of these black-body-like objects as photometric or spectrophotometric standards.

Such an object was found serendipitously while the quasar spectra in Baryon Acoustic Oscillation Spectroscopic Survey of SDSS-III (BOSS, Dawson et al. 2013) were visually inspected. This object was primarily targeted as a quasar candidate (Ross et al. 2012), but it does not resemble any type of quasars, and was eventually rejected from the quasar catalogue (Pâris et al. 2014). It turned out to be a star with a smooth-featureless spectrum. In fact, this object shows a proper motion, which, together with the close proximity in its spectrum, leads us to conclude that this is a star having a black-body spectrum.

We have then conducted a systematic search for such stars showing the black-body-like spectrum from the archived 4.3 million SDSS spectral objects. We select 22 stellar-like objects showing smooth black-body-like spectra. We then employ GALEX satellite data for ultraviolet photometry. We study if a black-body spectrum in the optical wavelengths continues to UV. Particularly, it is important to find the peak and turnover of the black-body spectrum in the UV region: we drop one star that does not pass this test. We finally employ WISE satellite data for infrared photometry. It is amazing to see that the majority of the stars we found for black-body-like star candidates show spectra that extrapolate smoothly to the infrared as far as  $3.4\mu\text{m}$ . It is known that some stars, specifically white dwarfs, are occasionally surrounded by a disc or dust debris that exhibits some IR excess (Debes et al. 2011). We carried out this test: 17 objects survived, and we present these objects as black-body stars in this paper. We dropped four objects that show an IR excess from our sample.

We may use these black-body-like stars for the photometric standard for the verification of the photometric system across various photometric passbands, to the accuracy that they are indeed black-body stars. This enables us to examine photometric systems used in the literature, in particular the accuracy of the zero points, across various photometric bands, which otherwise cannot easily be carried out. This also allows us to examine possible relative consistency among a few photometric systems that adopt the ‘AB system’ outside the optical passband used in different projects. These black-body stars can also be used as standard stars for photometric and spectrophotometric observations. Our objects all range in 17–19th mag in the  $r$  band, which is appropriate for standard stars for 8–10 metre telescopes.

## 2. Data and Search for Black-Body Stars

### 2.1. SDSS

Our primary source is the spectroscopic data archive of SDSS in DR7 (Abazajian et al. 2009) and DR12 (Alam et al. 2015). There are little overlaps in targets between the two data sets, while the spectrograph was modified between the two. After DR7, the final data release of the SDSS I and II projects, the spectrograph has been modified for SDSS-III: the wavelength range has widened, the fibre aperture size was narrowed, and washers are installed to correct for a tilt against the focal plane in the spectrograph to enhance the signal-to-noise ratio in blue wavelengths, while sacrificing the quality of the flux calibration (Dawson et al. 2013).

In the SDSS data reduction spectrophotometric flux is integrated over the filter curve and calibrated against its broad-band, point-spread-function (PSF) photometry of stars. We confirmed that spectrophotometric flux agrees with broad-band photometry within a 1% systematic difference with an rms scatter, however, of 7% in the  $g$ -,  $r$ - and  $i$ -bands. We remark here that the precision of broadband photometry is typically 1% for the  $g, r, i, z$ -bands and 2% for the  $u$ -band, as claimed in the DR7 SDSS document. Spectroscopic flux is then calibrated against the model of Gray et al. (2001) for spectrophotometric standard stars per spectroscopic plate, typically F subdwarfs, as described in the SDSS DR6 paper (Adelman-McCarthy et al. 2008).

The observed spectra are automatically classified into object types by the SDSS pipeline (Bolton et al. 2012). The majority of the objects are correctly classified, but classification into ‘quasars’, often suffers from contaminations of other types of objects, or sometimes redshift mis-measured, by a few percent probability. Visual inspection is conducted for all spectra classified as “Quasar”.

Quasars and white dwarfs often have similar colours, resembling the black-body spectrum. Hence, many white dwarfs and the targets we are looking for are included in the candidate quasar sample in the target selection of SDSS. We go back to the master data archives. The essential initial step of our work is to search for featureless spectra with rather close to black-body in the data archive of SDSS-I/II (Data Release 8, Aihara et al. 2011) and SDSS-III (Data Release 12, Alam et al. 2015). We use the data reduction version of v5.3.12 for DR8, and v5.7.0 for DR12. We examine 1,843,200 spectra in DR8 and 2,463,000 spectra in DR12. We fit the black-body spectrum to all spectra with two free parameters, the effective temperature and a flux normalization factor. We did not introduce reddening or a spectral tilt at this stage. We preselect spectra with  $S/N > 20$  per pixel at the  $r$ -band wavelength to avoid noisy spectra that would obscure absorption features. We collect objects whose reduced  $\chi^2/\text{dof}$  of the black-body fit is less than 1.05. We find 465 objects from the total of 798,593 star-like objects. We find that the effective temperature is roughly 10,000K for most of the objects we are looking for. Then, we visually inspected all 465

objects and rejected ones that show absorption features. We remark that DC white dwarf is defined as a star with featureless spectrum with the strength of the absorption lines less than 5% of its continuum. We rejected spectra with H or He absorption lines if they are visible, if weak, within the allowed S/N of the SDSS data. 22 stars survived this selection.

Once we identify candidates for featureless objects with spectra close to the black-body in the spectral archives, we employ the five broad-band photometry data from SDSS DR8 to enhance the photometric accuracy in the optical band. We remark that DR8 presents the last release of photometry of SDSS and includes all SDSS objects<sup>1</sup>. After confirming that the photometric data are consistent with spectrophotometry, we refit to obtain the temperature and the flux normalization from broad-band photometry, whereas we should wait for the introduction of the GALEX UV data to give more definitive temperatures.

SDSS photometry is designed to be in the AB magnitude system. It is constructed based on the absolute flux of  $\alpha$  Lyr (Vega), and used spectrophotometry of BD+17°4708 as the intermediary. Slight offsets, however, are claimed in order to make it closer to the AB system in SDSS photometry. For example it is suggested in their data release paper (say DR8) that some offset be added to the values given in the SDSS photometry data release for DR7 and DR8: AB–SDSS=  $-0.042, +0.036, +0.015, +0.013$  and  $-0.002$ <sup>2 3</sup> for  $u, g, r, i, z$ -bands from SDSS magnitude to (pseudo)AB magnitude. It is one of our purposes to examine the validity of this possible offset, as seen in the next section.

## 2.2. GALEX

We extend our study to include the UV using the all-sky survey of GALEX (Morrissey et al. 2007). We fit a black-body spectrum to these spectral energy distributions (SED) in addition to those of SDSS, both taking broad-band photometry, and examine if the fit is consistent with black-body fitted to the optical band alone.

We collect the photometric data for FUV ( $\lambda$ 1350-1780) and NUV ( $\lambda$ 1770-2730). GALEX

---

<sup>1</sup>The data in DR8 occasionally differ from those in DR7 due to the re-reduction the data by the SDSS team. The difference between the two data releases is typically of the order of 0.01 mag in either positive and negative way, but it amounts for some cases to 0.05 mag. The difference does not seem to show any systematic trends

<sup>2</sup>These offsets are being used in the SDSS pipeline routine named “SDSSFLUX2AB” in their IDL package. It was derived by David Hogg (2003, private communication).

<sup>3</sup>IDL package can be found in : [https://users.obs.carnegiescience.edu/yshen/IDL/photoop\\_doc.html](https://users.obs.carnegiescience.edu/yshen/IDL/photoop_doc.html)

photometry has been calibrated to STScI CALSPEC (Bohlin et al. 2001) in its AB magnitude system. GALEX photometry is important for our project to find the turnover of black-body spectra when temperature is  $< 20,000$  K, which is indicated in our fit to the optical spectrum. One candidate star, J121886+414800, does not show a turn over in UV, so is dropped from our black-body star sample. This makes our sample 21 stars. We derive the effective temperature and flux normalization factor from fit to the photometric data of SDSS and GALEX, which are shown in Table 1 below. We reserve for a possibility in mind that the zero point of the AB magnitude of GALEX may deviate from that of the SDSS AB photometric system.

We also check for the proper motion of black-body candidate stars (Roeser et al 2010). We should reject candidates when they exhibit no proper motions. They might be candidates for BL Lac objects. All our 22 candidate objects, however, show significant proper motions of the order of 20–70 mas/yr per coordinate, which is consistent with their distances tens of parsec. This distance is consistent with distance moduli inferred from brightness and general luminosity if these stars are white dwarf like objects. In any case, we conclude that these stars are in the local field.

### 2.3. WISE

We supplement our study with infrared photometry of WISE, which has observed the sky at 3.4, 4.6, 12 and 22  $\mu\text{m}$  (W1, W2, W3 and W4 filters, respectively) (Wright et al. 2010). We use the photometric catalogue of Lang et al. (2016), which introduced “forced” photometry, where the positions of objects are fixed to those in SDSS photometry, and unblurred images are coadded (unWISE) to deepen the survey depth<sup>1</sup>. Only the W1 (3.4 $\mu\text{m}$ ) channel is appropriate to our work, for photometry matches the depth we require only in this passband. WISE photometry is presented taking  $\alpha$  Lyr (Vega) as the zero magnitude. This is transformed to the AB system using the conversion given in Wright et al. (2010). We reserve here again for a possibility of mismatch in the zero point of AB photometry between WISE and SDSS. We remark that the original WISE data release does not reach the depth we need.

It has been known that a significant fraction (say, 20%) of white dwarfs have dust debris around the star that is manifested as an IR excess (Debes et al 2011). The IR data are essential to rule out objects with the IR excess. We find that 4 among 22 objects show a significant IR excess, and drop them from our sample of black-body stars. This makes our final sample to be 17. For this sample, the black-body fit from the UV to the optical region extrapolates well to 3.4 $\mu\text{m}$ .

---

<sup>1</sup>We thank Brice Ménard for his suggestion to use forced photometry to increase the depth to match our study.

### 3. Result

Our initial 22 black body star candidates are presented in Table 1. It includes 4 stars showing the IR excess and one star that does not fit GALEX UV. We carry out global black-body fits to the available broad-band photometric data of SDSS and GALEX. The fit parameters are  $T_{\text{eff}}$  and the flux normalization factor  $a$ , as:

$$f_{\lambda} = a \frac{2hc^2}{\lambda^5} \frac{1}{\exp(hc/\lambda kT_{\text{eff}}) - 1} \quad (1)$$

where  $\lambda$  is the wavelength,  $h$  the Planck constant and  $k$  is the Boltzmann constant. The normalization  $a$  is a dimensionless factor and given in this table as well as  $\chi^2/\text{dof}$ . We do not introduce extinction corrections in this fit. The normalization factor is alternatively represented as the angular size  $\theta$ ,

$$\theta = \frac{R}{d} = \sqrt{\frac{f_{\nu}(T_{\text{eff}})}{\pi B_{\nu}(T_{\text{eff}})}} = \sqrt{\frac{a}{\pi}}, \quad (2)$$

where  $B_{\nu}(T_{\text{eff}})$  is the Planck radiation brightness,  $R$  is the radius, and  $d$  is the distance to the star.

In Figure 1 we present the spectra of the 22 stars given in Table 1 and the fits to the black-body spectrum. We include one star with its UV deviated from GALEX. The fit is carried out without using WISE photometry as a constraint. This then shows that the IR excess is apparent for four stars beyond 2 sigma. When an IR excess is not apparent, the fit from optical spectra extrapolates well to IR 3.4 $\mu\text{m}$  (within 1.2 sigma), which corroborates the conclusion that the emission from the stars is close to black-body. To scrutinize the deviation from the black-body spectrum, we show in the lower panels the residual of the observed flux against the black-body fit given in the fraction. For WISE W1 we show this separately, as its error is too large to display in the same scale as other bands. We are left with 17 black-body stars. Note that chi squares are not necessarily good for some stars, so that one may further reject some depending on their purpose.

We note that the temperature and the normalization are correlated in the fit. We demonstrate an example for J124535.626+423824.58 in Figure 2, where thick-hatched region is the 1  $\sigma$  allowed range in the fit to the SDSS data only. This is squeezed to a thicker-hatched region upon the use of the GALEX data, resulting in the reduced temperature error of  $\pm 50\text{K}$ . The inclusion of WISE does not improve the result. This trend differs little for the other 16 stars.

The black-body fit and the residuals are shown in Table 2: the residuals are also plotted in Figure 3(a). Brightness given in Table 2, assuming that the emission is perfect black-body, may be used as the photometric standard, till more accurate observation becomes available. We added our calculation for the  $J$ ,  $H$ , and  $K$  bands of Subaru MOIRCS (Suzuki et al. 2008) and W1 for WISE. NIR is not used as a constraint to the fit. The zero-point is SDSS pseudo-AB system. The mean residuals over our 17 stars are given in the upper row of Table 3. For the optical bands, they

are all consistent with zero within errors of 0.01 mag, smaller than the typical error of  $u$  or  $z$  band photometry. This means that the SDSS photometry zero points are consistent across the  $u$  to the  $z$  bands: no appreciable deviations are seen in the zero-point of any of the five passbands. We also see that deviations are of random nature without showing systematic trends. Looking at the deviations star-by-star, there seems no apparent correlations between colour bands. The same can be said for GALEX NUV. There seems no offset in the GALEX zero point against the SDSS AB system beyond the photometric scatter. The deviation is recognizable for GALEX FUV: observed brightness is fainter by 0.1-0.2 mag than the black-body, while the large photometric scatter does not allow us to draw a precise conclusion. For W1 of WISE, the offset of mean is  $0.452 \pm 0.663$ . The error is large, while it is consistent with zero. We note that we use forced photometry of WISE and we do not use WISE W1 as a constraint to fit to the black-body. We cannot derive an accurate conclusion as to the zero point of WISE photometry.

It has been alleged that SDSS photometry is deviated from the AB system and some offsets should be added to the bare value of SDSS photometric pipeline output<sup>1</sup>. We compare SDSS photometry to that with the suggested offsets (as given in the bottom of Sect. 2.1) added to the data, and re-minimize the black-body fit that is given in row 3 of Table 3. This is also shown in panel (b) of Figure 3. We now see the residuals increased significantly, in particular in the  $u$  band, where a rather large offset ( $-0.042$  mag) is added. The residual to the black-body seen in this figure looks somewhat larger and also wiggly across the five colour bands: the observed is brighter in  $u$  and fainter in  $g$ .

We also compare SDSS photometry to photometry with the AB zero point set by CALSPEC (Holtzman et al. 2008), by re-minimizing again the entire fit, as shown in row 5 in Table 3<sup>2</sup>, and also in panel (c) of Figure 3. We observe a wiggle similar to the plot with Hogg's offset above, indicating brighter  $u$  and fainter  $g$ . Departures of residuals from zero are larger in the  $u$  and  $z$  bands, 0.038 mag, and  $-0.027$  mag, respectively, which are compared to  $< 0.01$  mag offsets with the original magnitude system of SDSS. We conclude that original SDSS photometry works better than adding some offsets or using the CALSPEC standard as the AB zero magnitude.

We see in these Figure and Table that GALEX NUV photometry smoothly matches SDSS photometry, to the level of a few times 0.01 mag, albeit the scatter of photometry in the NUV band is as large as 0.08 mag, verifying the consistency between the SDSS photometric system and GALEX NUV. For FUV photometry a large scatter of the order of 0.1 mag seen in our residual figure hinders us from deriving an accurate conclusion as to the zero point offset, but the mismatch

---

<sup>1</sup>This has been claimed by David Hogg (private communication) and is used in some analyses, in particular of spectrophotometric data handling, of SDSS.

<sup>2</sup>The constant added is  $-0.037$  ( $u$ ),  $0.024$  ( $g$ ),  $0.005$  ( $r$ ),  $0.018$  ( $i$ ) and  $-0.016$  ( $z$ )

of the AB magnitudes between the two systems is at most of the order of 0.2 mag. Our finding here indicates that these stars can be used as spectrophotometric standards from UV to IR with expected errors and fluctuations in mind.

Our fit gives the temperature of our black-body stars 8500 to 12000K. So we may conclude that these stars are consistent with DB white dwarfs with He lines undeveloped. The white dwarf spectrum is generically not very far from the black-body spectrum up to absorption features. If we assume that these black-body stars are white dwarfs, the observed brightness indicates the distance to be roughly of the order of 50 pc. This is also consistent with the distance indicated by large proper motions. A typical distance of 50 pc in the Galactic disc indicates extinction  $E(B - V) \approx 0.01$  or  $A_r \approx 0.03$  mag. Note that we cannot estimate the distance from colours. We also note that dust reddening is almost parallel to the temperature in colour space. The reddening correction modifies the resulting temperature, but, as we confirmed, the residuals of the black-body fits are modified very little, only up to 0.01 mag even for a very large extinction,  $E(B - V) = 0.10$ . Therefore, our conclusion as to black-body stars is not modified. The fitted temperature becomes lower as  $\Delta T \approx 122[E(B - V)/0.01]K$  upon the inclusion of reddening.

#### 4. Conclusion

We have discovered 17 stars that show spectra very close to the black-body for a wide range of spectrum from GALEX FUV to the IR  $\lambda = 3.4\mu\text{m}$  band out of 4,300,000 spectra archived in the SDSS data base. These spectra can give us a unique possibility to examine the magnitude system, in particular the zero point of the photometric system in AB, across the various colour bands within SDSS, or even across the different system used by GALEX against that of SDSS, or WISE versus SDSS. Within the SDSS photometric system, we would indicate that the zero point of the 5 colour bands is consistent within 0.01 mag. We do not find indication for the offset with SDSS AB photometry up to the absolute constant common in the 5 bands. We do *not* need to introduce any additional constant to adjust to the ‘AB system’. GALEX NUV photometry zero point is consistent with SDSS photometric zero point within a few hundredths of mag, although large scatter of NUV photometry ( $\approx 0.07$  mag) hinders from a more accurate conclusion. During this study we also noted a 0.02–0.04 mag error in the optical zero point of the CALSPEC AB standard.

The black-body stars we found are as faint as 17–19 mag in  $r$ , and can be used as photometric, but also as spectrophotometric standard stars for the work with large aperture telescopes. We consider that these stars in our sample are consistent with DB white dwarfs with temperature around 10000 K.



## Acknowledgment

We thank Brice Ménard for useful discussion and Ting-Wen Lan for assisting us to collect the WISE data. NS is partially supported by JST CREST JPMHCR1414 and JSPS Programs for Advancing Strategic International Networks to Accelerate the Circulation of Talented Researchers. MF thanks Hans Böhringer and Yasuo Tanaka for the hospitality at the Max-Planck-Institut für Extraterrestrische Physik and also Eiichiro Komatsu at Max-Planck-Institut für Astrophysik, in Garching. He also wishes his thanks to Alexander von Humboldt Stiftung for the support during his stay in Garching, and Monell Foundation in Princeton. He received in Tokyo a Grant-in-Aid (No. 154300000110) from the Ministry of Education. Kavli IPMU is supported by World Premier International Research Center Initiative of the Ministry of Education, Japan.

## REFERENCES

- Abazajian, K. N., Adelman-McCarthy, J. K., Agüeros, M. A., et al. 2009, *ApJS*, 182, 543 (DR7)
- Adelman-McCarthy, J. K., Agüeros, M. A., Allam, S. S., et al. 2008, *ApJS*, 175, 297 (DR6)
- Aihara, H., Allende Prieto, C., An, D., et al. 2011, *ApJS*, 193, 29 (DR8)
- Alam, S., Albareti, F. D., Allende Prieto, C., et al. 2015, *ApJS*, 219, 12 (DR12)
- Bohlin, R. C., Dickinson, M. E., Calzetti, D., 2001, *AJ*, 122, 2118
- Bolton, A. S., Schlegel, D. J., Aubourg, É., et al. 2012, *AJ*, 144, 144
- Dawson, K. S., Schlegel, D. J., Ahn, C. P., et al. 2013, *AJ*, 145, 10
- Debes, J. H., Hoard, D. W., Wachter, S., Leisawitz, D. T., & Cohen, M. 2011, *ApJS*, 197, 38
- Gray, R. O., Graham, P. W., & Hoyt, S. R. 2001, *AJ*, 121, 2159
- Holtzman, J. A., Marriner, J., Kessler, R. et al. 2008, *ApJ*, 136, 2320
- Lang, D., Hogg, D. W., & Schlegel, D. J. 2016, *AJ*, 151, 36
- Morrissey, P., Conrow, T., Barlow, Tom., et al. 2007, *ApJS*, 173, 682
- Pâris, I., Petitjean, P., Aubourg, É., et al. 2014, *A&A*, 563, A54
- Roeser, S., Demleitner, M., & Schilbach, E. 2010, *AJ*, 139, 2440
- Ross, N. P., Myers, A. D., Sheldon, E. S., et al. 2012, *ApJS*, 199, 3

Suzuki, R., Tokoku, C., Ichikawa, T., et al. 2008, PASJ, 60, 1347

Wright, E. L., Eisenhardt, P. R. M., Mainzer, A. K., et al. 2010, AJ, 140, 1868

Table 1. 22 Black-body Candidates: Coordinates and Photometric Data

SDSS name	RA (J2000)	DEC (J2000)	GALEX FUV	GALEX NUV	SDSS u	SDSS g	SDSS r	SDSS i	SDSS z	WISE W1	T (K)	$\alpha(\times 10^{-23})$	$\theta(\times 10^{-9})$	$\chi^2/\text{dof}$
J002739.497-001741.93	00:27:39.497	-00:17:41.93	21.80±0.06	19.89±0.02	19.05±0.02	18.90±0.03	18.98±0.02	19.12±0.03	19.37±0.05	21.21±0.48	10662±60	0.435±0.010	242.7±2.8	0.84
J004705.818-004820.09*	00:47:05.818	-00:48:20.09	20.02±0.04	19.29±0.02	19.00±0.03	19.01±0.02	19.24±0.02	19.50±0.02	19.60±0.05	21.07±0.41	14648±94	0.164±0.003	149.0±1.6	8.67
J004830.324+001752.80	00:48:30.324	+00:17:52.80	21.18±0.05	19.14±0.01	18.27±0.03	18.14±0.01	18.23±0.01	18.38±0.01	18.63±0.03	20.46±0.22	10639±40	0.876±0.013	344.5±2.5	5.10
J014618.898-005150.51	01:46:18.898	-00:51:50.51	20.61±0.05	18.80±0.01	18.21±0.02	18.17±0.02	18.24±0.01	18.42±0.01	18.61±0.03	21.19±0.41	11770±48	0.672±0.010	301.8±2.3	8.52
J022936.715-004113.63	02:29:36.715	-00:41:13.63	23.04±0.14	20.73±0.01	19.38±0.03	19.07±0.03	19.09±0.01	19.17±0.02	19.31±0.04	21.00±0.30	8901±31	0.640±0.011	294.5±2.5	1.93
J083226.568+370955.48	08:32:26.568	+37:09:55.48			19.39±0.03	18.98±0.01	18.84±0.03	18.83±0.02	18.93±0.04	20.63±0.24	7952±95	1.137±0.050	392.4±8.5	0.63
J083736.557+542758.64	08:37:36.557	+54:27:58.64			19.24±0.03	18.73±0.03	18.56±0.02	18.54±0.02	18.52±0.04	20.34±0.16	7449±61	1.815±0.055	495.8±7.5	3.38
J100449.541+121559.65	10:04:49.541	+12:15:59.65			19.41±0.02	19.18±0.03	19.23±0.02	19.32±0.02	19.43±0.05	22.25±1.07	9773±136	0.440±0.019	244.1±5.2	0.57
J103123.906+093657.89*	10:31:23.906	+09:36:57.89			18.73±0.03	18.64±0.02	18.80±0.01	18.96±0.02	19.15±0.05	20.63±0.25	11667±224	0.419±0.020	238.2±5.7	0.40
J104523.866+015721.96	10:45:23.866	+01:57:21.96			19.32±0.03	19.09±0.01	19.01±0.01	19.07±0.02	19.28±0.07	22.13±1.04	8956±87	0.666±0.021	300.3±4.7	2.56
J111720.801+405954.67	11:17:20.801	+40:59:54.67	20.93±0.34	18.98±0.09	18.26±0.02	18.08±0.01	18.19±0.01	18.34±0.01	18.63±0.04	23.00±1.91	10950±121	0.843±0.026	337.9±5.1	2.56
J114722.608+171325.21	11:47:22.608	+17:13:25.21			18.91±0.03	18.65±0.02	18.68±0.02	18.83±0.02	19.00±0.04	22.24±1.06	9962±109	0.669±0.022	301.0±4.9	1.92
J121856.693+414800.29 <sup>a</sup>	12:18:56.693	+41:48:00.29	17.59±0.06	17.84±0.04	17.91±0.02	18.18±0.02	18.62±0.02	18.90±0.01	19.22±0.05	22.58±1.26	23357±383	0.133±0.004	134.7±2.0	7.03
J124535.626+423824.58	12:45:35.626	+42:38:24.58			17.32±0.02	17.14±0.02	17.18±0.02	17.29±0.01	17.46±0.02	19.60±0.08	10086±67	2.650±0.057	599.1±6.4	0.17
J125507.082+192459.00	12:55:07.082	+19:24:59.00			18.83±0.04	18.53±0.02	18.45±0.01	18.50±0.01	18.63±0.03	21.75±0.78	8882±98	1.157±0.039	395.8±6.6	1.46
J134305.302+270623.98	13:43:05.302	+27:06:23.98			19.05±0.02	18.93±0.02	19.00±0.02	19.14±0.02	19.34±0.07	22.09±0.85	10678±151	0.427±0.017	240.4±4.8	0.20
J135816.735+144202.27*	13:58:16.735	+14:42:02.27	21.93±0.12	19.46±0.02	18.34±0.03	18.06±0.03	18.02±0.02	18.07±0.01	18.12±0.03	19.77±0.09	9191±44	1.598±0.030	465.2±4.3	3.39
J141724.329+494127.85	14:17:24.329	+49:41:27.85	20.73±0.29	18.27±0.06	17.36±0.03	17.25±0.03	17.31±0.02	17.43±0.02	17.61±0.03	20.01±0.08	10503±112	2.127±0.066	536.7±8.3	1.01
J151859.717+4002839.58	15:18:59.717	+40:02:839.58			19.71±0.03	19.44±0.01	19.37±0.02	19.51±0.03	19.57±0.07	21.57±0.47	9072±131	0.458±0.022	249.1±5.9	0.71
J161605.194+142116.70*	16:16:05.194	+14:21:16.70	22.32±0.47	19.57±0.07	18.70±0.02	18.61±0.01	18.70±0.01	18.85±0.02	19.02±0.04	19.52±0.07	10918±119	0.533±0.016	268.6±4.1	1.08
J161704.078+181311.96	16:17:04.078	+18:13:11.96			19.17±0.03	18.78±0.02	18.73±0.02	18.80±0.02	18.81±0.04	21.56±0.44	8568±88	0.996±0.034	367.2±6.2	2.00
J230240.032+003021.60	23:02:40.032	+00:30:21.60	20.79±0.06	18.88±0.01	17.97±0.02	17.80±0.02	17.90±0.02	18.02±0.02	18.25±0.03	21.19±0.42	10478±42	1.241±0.021	409.9±3.4	1.14

\* Stars that show IR excess. To be dropped from the list of black-body stars.

<sup>a</sup>GALEX UV data do not show turn-off. To be removed from the list of black-body stars.

Table 2. The best fit broad-band flux of the 17 black-body stars (upper rows) and the residuals from the fit (lower rows):  $\Delta m =$  Data—Black-Body in magnitude. Calculations are added for Subaru MOIRCS J, H, K and for W1 of WISE. NIR is not used as a constraint to the fit

Star name	GALEX FUV	GALEX NUV	SDSS-u	SDSS-g	SDSS-r	SDSS-i	SDSS-z	$\chi^2/\text{dof}$	MOIRCS-J	MOIRCS-H	MOIRCS-K	WISE W1
J002739.497-001741.93	21.705±0.027	19.905±0.010	19.041±0.002	18.911±0.007	18.980±0.010	19.124±0.012	19.306±0.014		19.753±0.015	20.170±0.016	20.647±0.017	21.470±0.018
	0.090±0.061	-0.017±0.019	0.010±0.022	-0.013±0.025	0.000±0.019	-0.005±0.034	0.060±0.034	0.84				-0.259±0.482
J004830.324+001752.80	20.965±0.019	19.158±0.008	18.289±0.000	18.158±0.003	18.225±0.006	18.368±0.007	18.550±0.008		18.996±0.009	19.413±0.010	19.889±0.010	20.712±0.011
	0.215±0.049	-0.021±0.027	-0.021±0.027	-0.017±0.014	0.007±0.014	0.007±0.014	0.082±0.014	5.10				-0.252±0.217
J014618.898-005150.51	20.351±0.018	18.839±0.007	18.169±0.001	18.121±0.004	18.250±0.006	18.425±0.007	18.630±0.008		19.108±0.010	19.541±0.010	20.031±0.011	20.867±0.011
	0.263±0.050	-0.040±0.012	0.045±0.019	0.046±0.019	-0.006±0.013	-0.004±0.015	-0.025±0.015	8.52				0.327±0.411
J022936.715-004113.63	23.126±0.020	20.716±0.007	19.450±0.001	19.140±0.005	19.079±0.008	19.155±0.010	19.289±0.011		19.668±0.012	20.049±0.013	20.498±0.013	21.293±0.014
	-0.086±0.144	0.009±0.012	-0.066±0.029	-0.065±0.031	0.008±0.015	0.012±0.017	0.025±0.017	1.93				-0.292±0.302
J083226.568+370955.48	23.824±0.097	20.972±0.048	19.420±0.017	18.977±0.002	18.819±0.009	18.844±0.015	18.942±0.019		19.270±0.024	19.624±0.027	20.053±0.030	20.827±0.032
			-0.025±0.031	0.008±0.015	0.026±0.028	-0.017±0.022	-0.013±0.022	0.63				-0.201±0.240
J083736.557+542758.64	24.149±0.073	21.016±0.037	19.286±0.014	18.757±0.003	18.538±0.005	18.530±0.009	18.604±0.012		18.899±0.016	19.235±0.018	19.651±0.020	20.412±0.022
	0.166±0.075	0.166±0.075	-0.045±0.026	-0.023±0.027	0.026±0.017	0.013±0.017	-0.081±0.162	3.38				-0.067±0.162
J100449.541+121559.65	22.541±0.092	20.461±0.046	19.411±0.015	19.199±0.002	19.209±0.008	19.322±0.013	19.482±0.017		19.898±0.022	20.299±0.025	20.763±0.027	21.573±0.029
			0.004±0.024	-0.019±0.025	0.021±0.023	0.000±0.021	-0.048±0.021	0.57				0.679±1.071
J104523.866+015721.96	23.016±0.071	20.629±0.036	19.377±0.013	19.074±0.002	19.018±0.005	19.096±0.009	19.232±0.012		19.614±0.016	19.996±0.018	20.446±0.020	21.242±0.021
			-0.053±0.028	0.021±0.010	-0.005±0.011	-0.024±0.016	0.050±0.016	2.56				0.886±1.038
J111720.801+405954.67	20.741±0.066	19.021±0.034	18.211±0.012	18.105±0.002	18.190±0.005	18.343±0.008	18.531±0.011		18.987±0.014	19.409±0.016	19.889±0.018	20.716±0.019
	0.186±0.336	-0.039±0.086	0.046±0.022	-0.027±0.013	0.002±0.014	-0.001±0.014	0.101±0.014	2.56				2.282±1.910
J114722.608+171325.21	21.893±0.071	19.877±0.036	18.869±0.012	18.676±0.002	18.699±0.006	18.819±0.010	18.985±0.013		19.408±0.017	19.812±0.019	20.279±0.020	21.092±0.022
		0.056±0.058	0.043±0.031	-0.027±0.016	-0.016±0.017	0.035±0.019	0.017±0.019	1.92				1.152±1.060
J124535.626+423824.58	20.276±0.042	18.300±0.020	17.319±0.006	17.138±0.000	17.170±0.005	17.295±0.007	17.463±0.009		17.891±0.011	18.297±0.013	18.767±0.014	19.581±0.015
			-0.000±0.017	0.001±0.017	0.015±0.019	-0.007±0.015	-0.004±0.015	0.17				0.022±0.081
J125507.082+192459.00	22.508±0.084	20.090±0.044	18.818±0.017	18.506±0.005	18.443±0.003	18.518±0.008	18.651±0.011		19.030±0.016	19.410±0.018	19.859±0.020	20.653±0.022
			-0.158±0.081	0.010±0.038	0.021±0.019	0.012±0.015	-0.025±0.015	1.46				1.100±0.781
J134305.302+270623.98	21.712±0.086	19.916±0.043	19.055±0.014	18.927±0.002	18.996±0.007	19.141±0.012	19.323±0.015		19.771±0.019	20.188±0.022	20.665±0.024	21.488±0.026
			-0.008±0.024	-0.002±0.021	0.005±0.016	-0.004±0.020	0.012±0.020	0.20				0.598±0.846
J141724.329+494127.85	20.124±0.066	18.277±0.033	17.382±0.011	17.238±0.001	17.297±0.006	17.436±0.009	17.615±0.012		18.057±0.015	18.471±0.017	18.946±0.019	19.766±0.020
	0.608±0.288	-0.008±0.056	-0.026±0.026	0.012±0.026	0.010±0.017	-0.005±0.022	-0.006±0.022	1.01				0.242±0.081
J151859.717+4002839.58	23.280±0.102	20.940±0.050	19.719±0.017	19.431±0.001	19.384±0.010	19.468±0.016	19.608±0.020		19.995±0.026	20.380±0.029	20.832±0.031	21.630±0.034
			-0.007±0.028	0.007±0.015	-0.013±0.016	0.040±0.033	-0.042±0.033	0.71				-0.057±0.473
J161704.078+181311.96	23.078±0.080	20.524±0.041	19.164±0.015	18.811±0.004	18.719±0.005	18.778±0.009	18.900±0.013		19.263±0.017	19.635±0.020	20.078±0.021	20.866±0.023
	0.074±0.123	0.006±0.025	-0.030±0.021	0.012±0.016	0.020±0.017	-0.092±0.017	-0.092±0.017	2.00				0.691±0.436
J230240.032+003021.60	20.731±0.020	18.877±0.007	17.977±0.001	17.831±0.005	17.889±0.007	18.027±0.009	18.205±0.010		18.646±0.011	19.060±0.012	19.534±0.012	20.354±0.013
	0.057±0.056	0.000±0.013	-0.009±0.021	-0.027±0.017	0.009±0.017	-0.002±0.020	0.041±0.020	1.14				0.838±0.422

Table 3. Mean of residuals from the black-body fit ( $\Delta m = \text{data} - \text{black-body fit}$ ): The 17 black-body stars are used in this calculation. Row 1 is with the raw value of brightness given in SDSS data release DR8; Row 2 gives the offsets suggested by Hogg to make the SDSS magnitude closer to the AB system, and row 3 is the mean residuals for this case. Row 4 gives the offsets suggested by Holzman (2009) to make the SDSS magnitude closer to the AB system with CALSPEC, and Row 5 is the mean residuals.

Data Name	GALEX FUV	GALEX NUV	SDSS-u	SDSS-g	SDSS-r	SDSS-i	SDSS-z
Mean Residuals without Offset	0.191±0.202	-0.000±0.081	-0.006±0.031	-0.008±0.025	0.007±0.012	0.002±0.017	0.003±0.052
Hogg's Offset to SDSS			-0.042	0.036	0.015	0.013	-0.002
Mean Residuals with Hogg Offset	0.218±0.215	0.016±0.097	-0.047±0.034	0.020±0.025	0.007±0.014	-0.002±0.016	-0.019±0.054
Holtzman et al Offset (CALSPEC)			-0.037	0.024	0.005	0.018	-0.016
Mean Residuals with Holtzman Offset	0.215±0.213	0.018±0.093	-0.038±0.033	0.013±0.025	0.003±0.013	0.009±0.016	-0.027±0.054

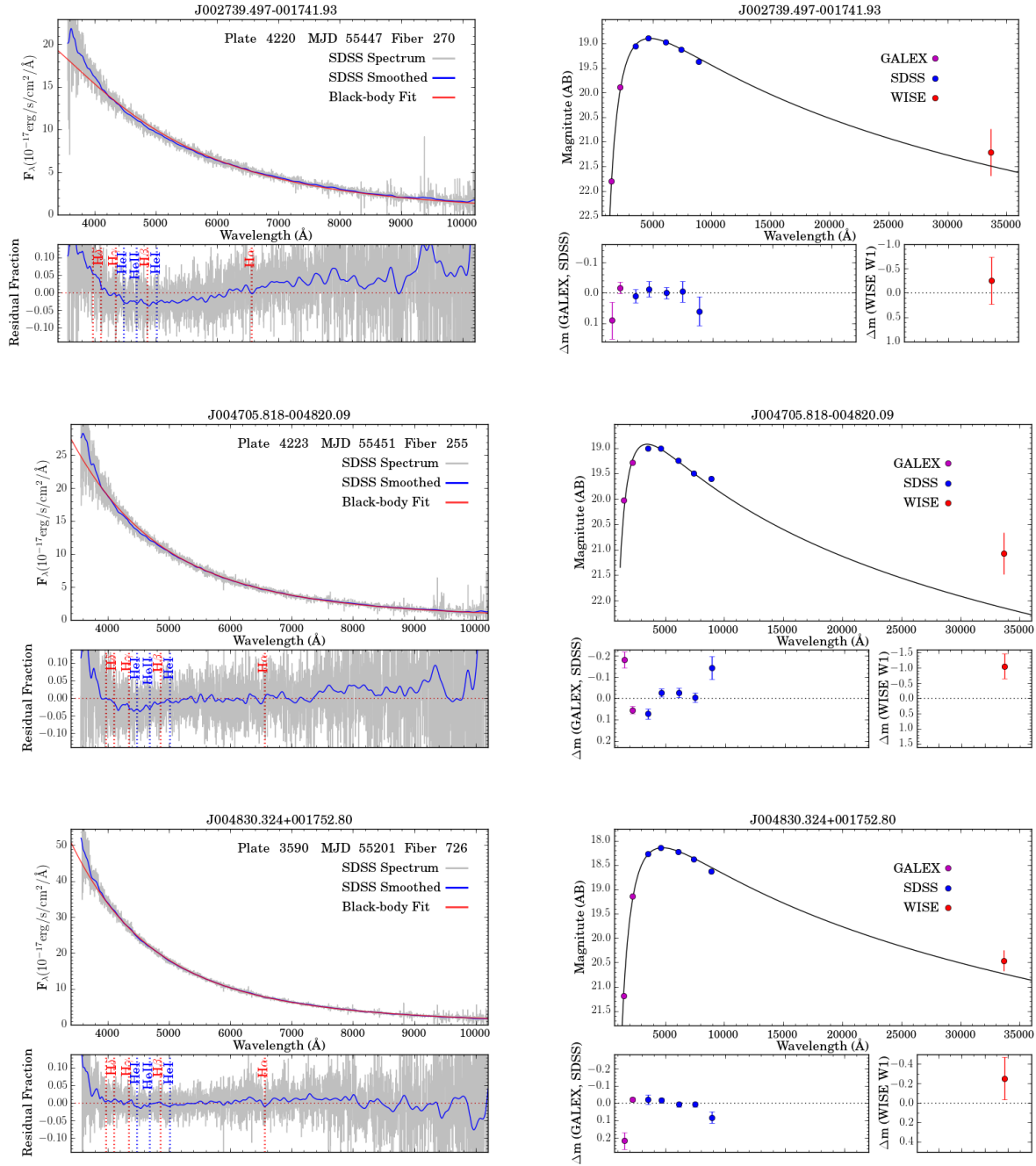
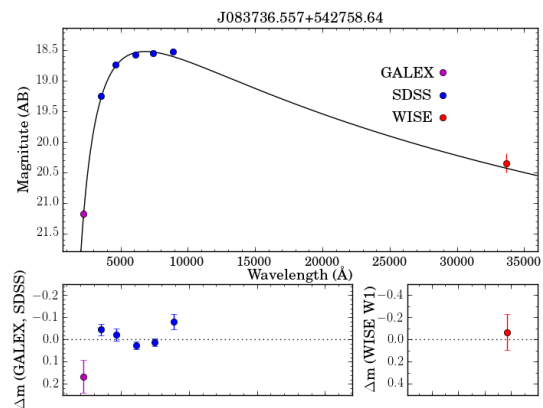
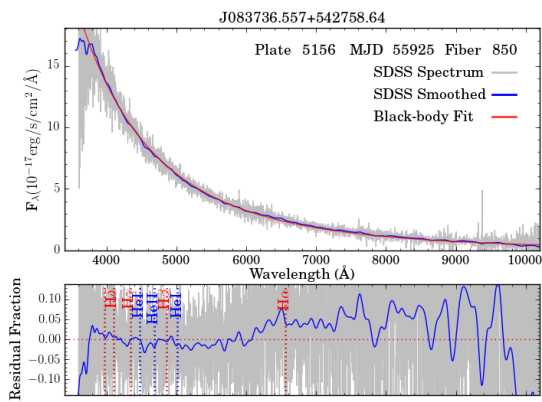
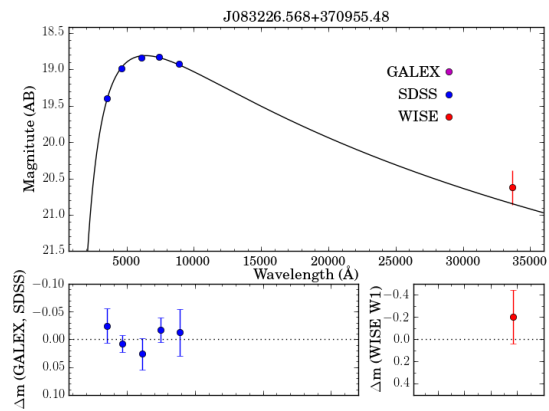
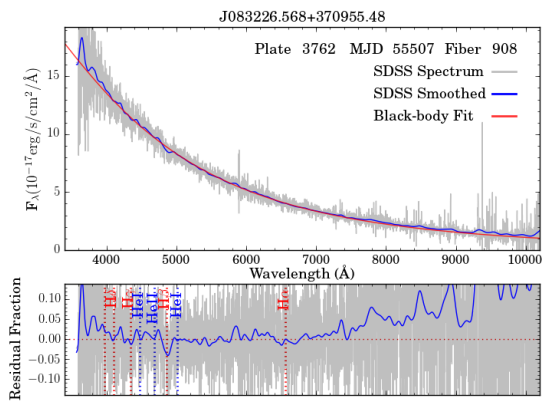
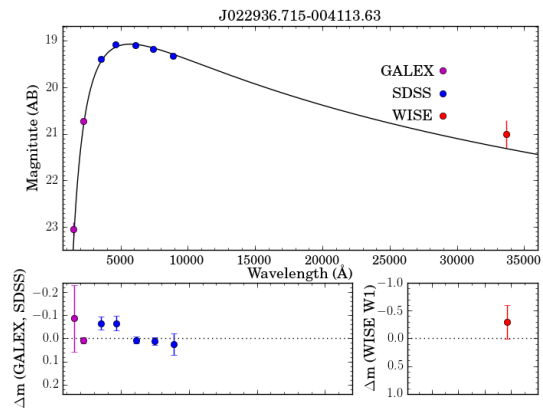
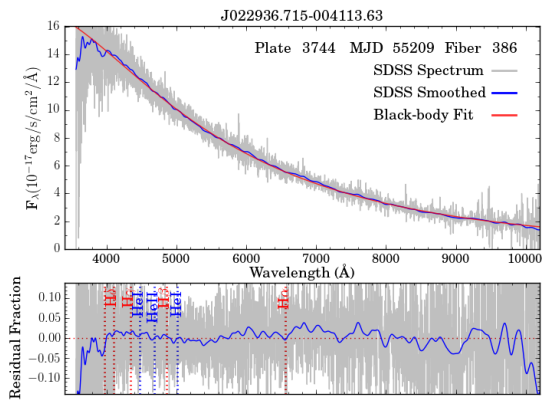
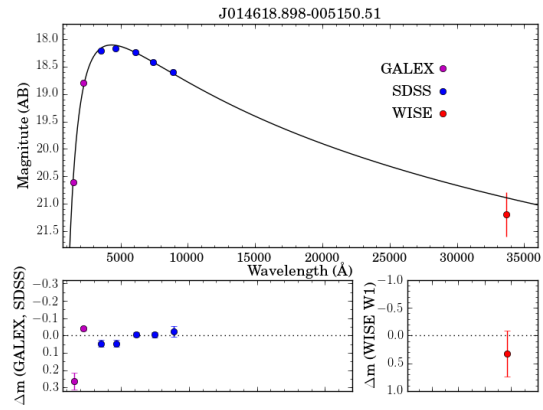
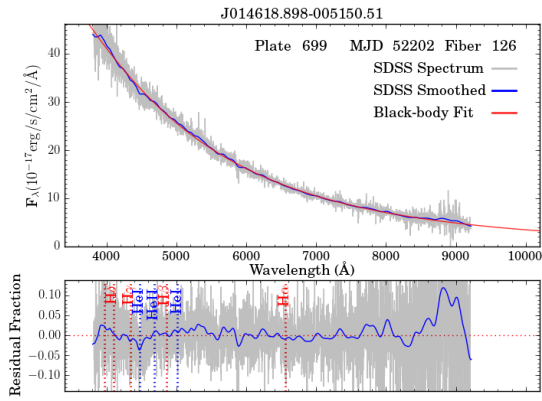
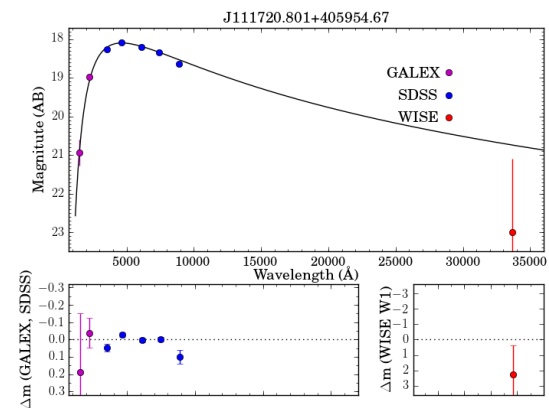
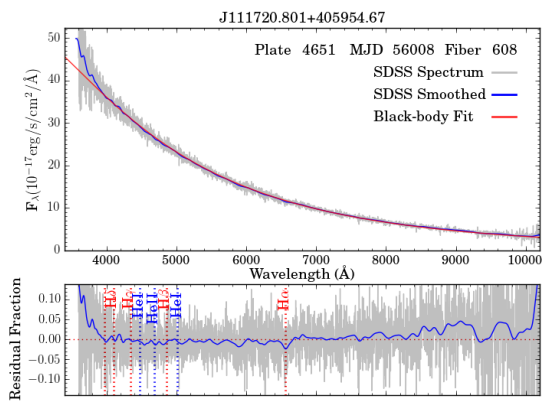
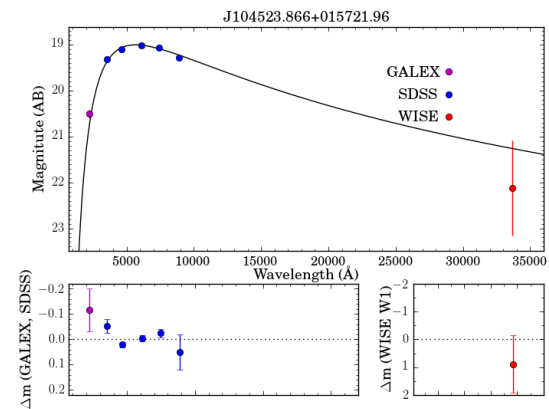
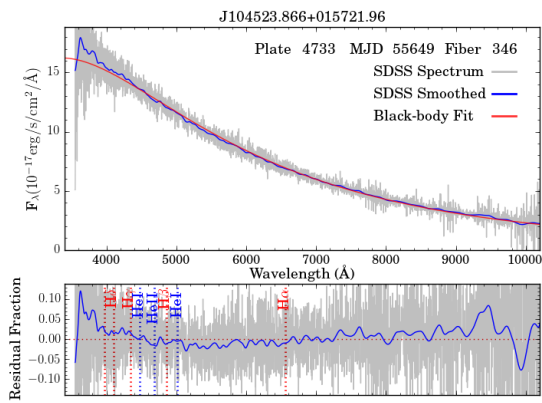
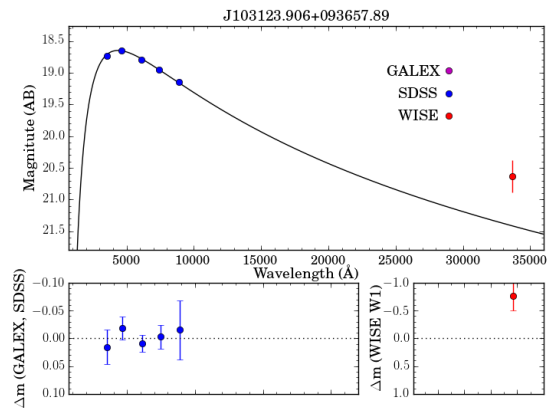
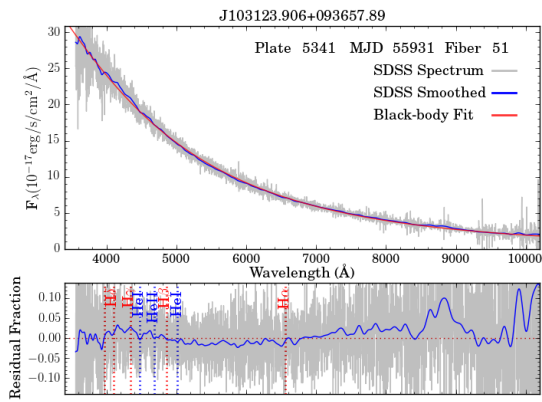
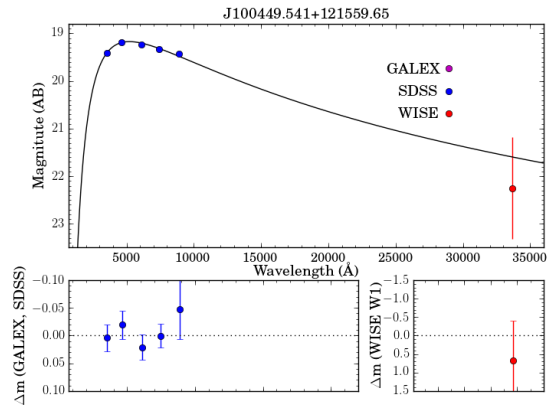
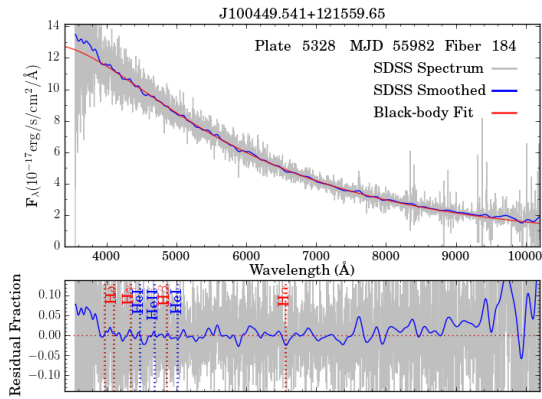
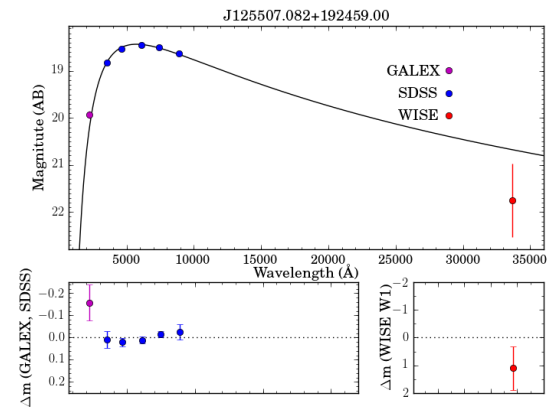
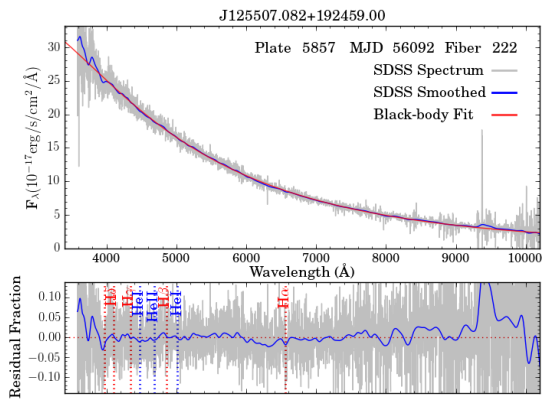
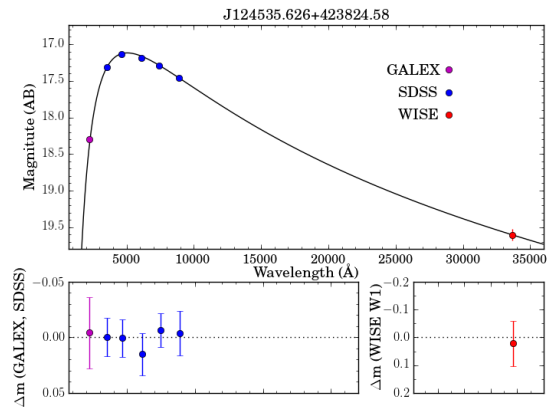
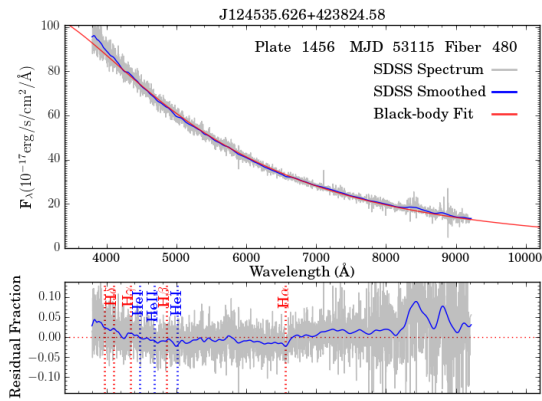
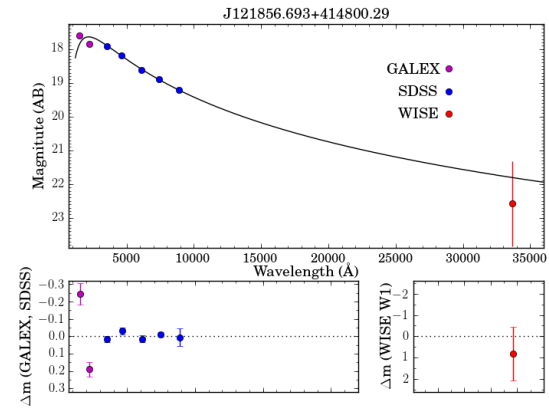
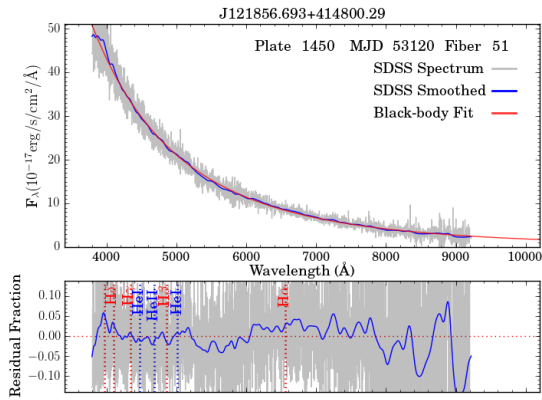
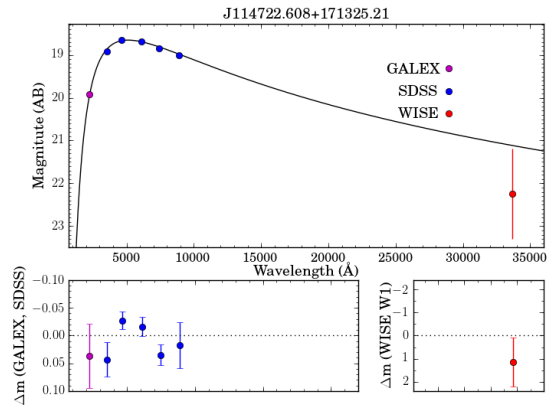
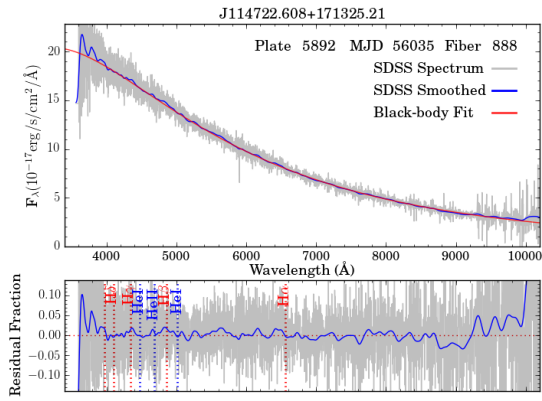


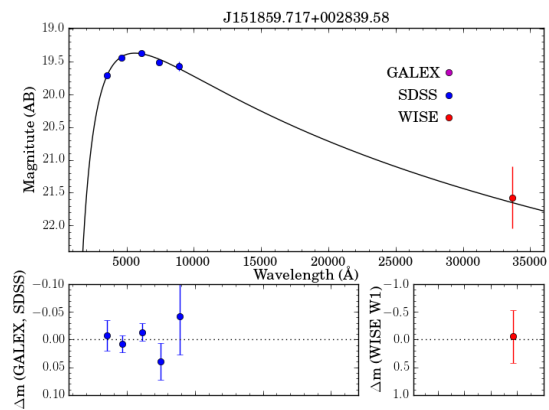
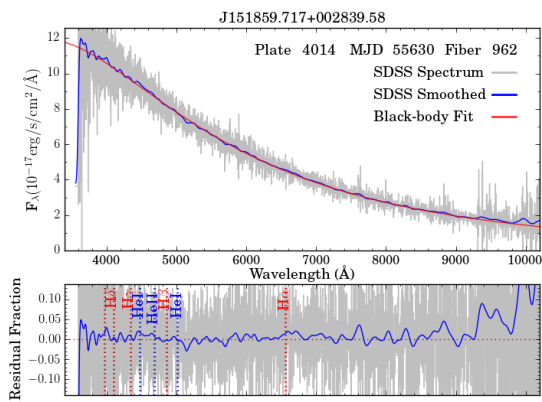
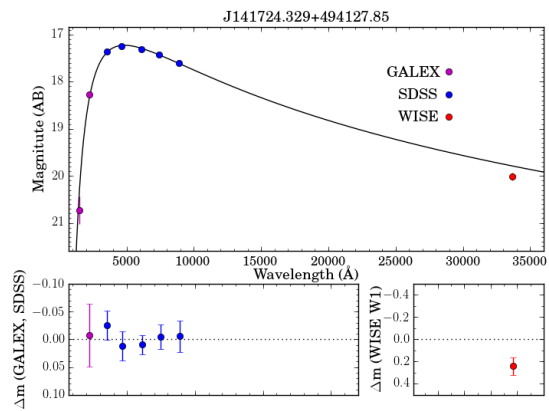
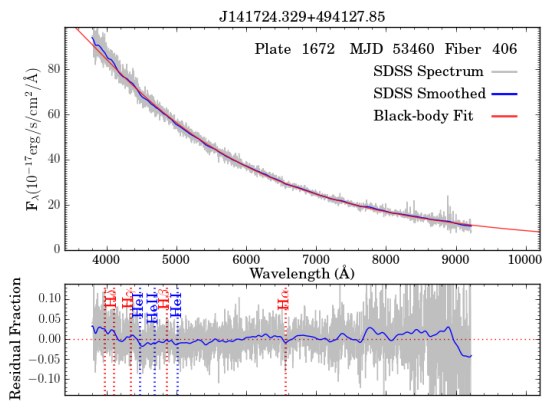
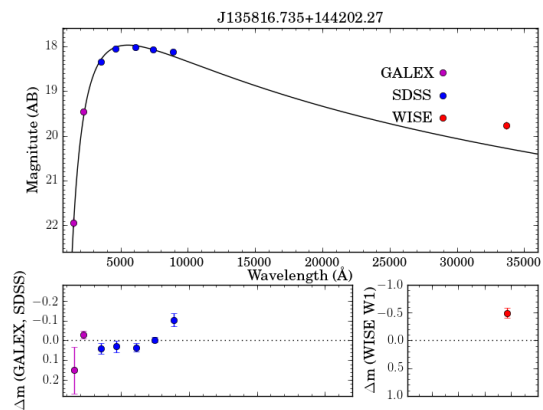
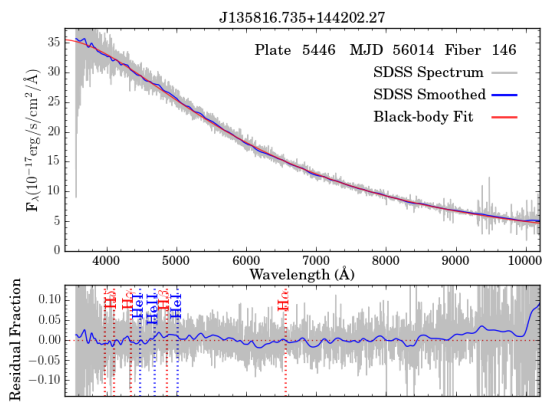
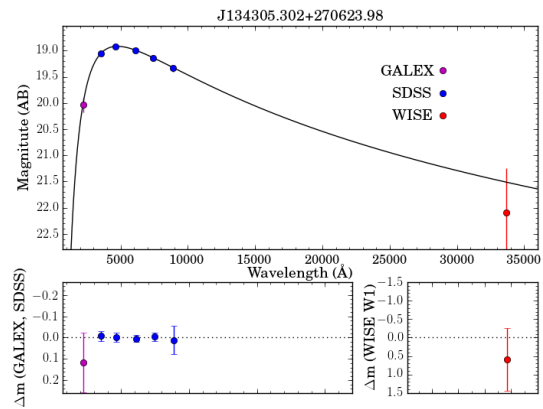
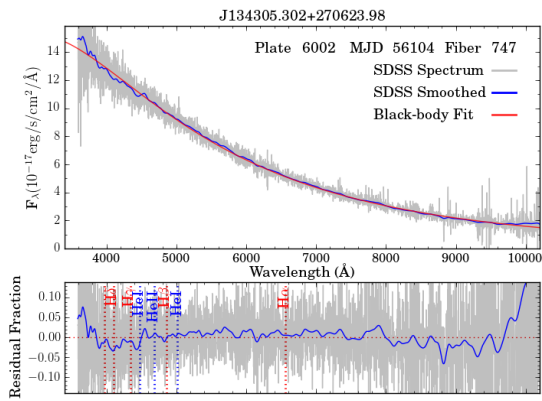
Fig. 1.— Spectra of 22 black-body star candidates. In the left panels, observed spectra are indicated with grey, and blue curves show smoothed spectra. Black-body fits are indicated with red. The right panels show their photometric data from which our fit parameters are derived. In the bottom panel, the residuals (fractional values) from the fits are shown, with the positions of hydrogen and helium absorption lines indicated.

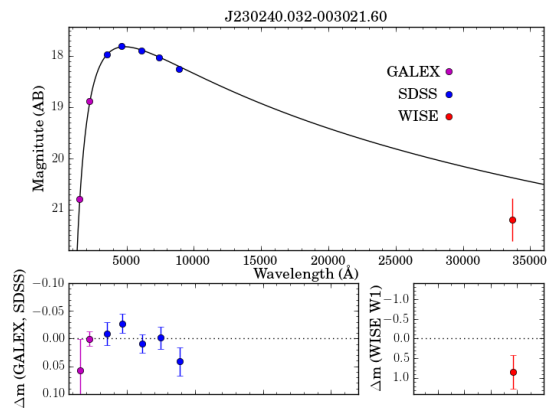
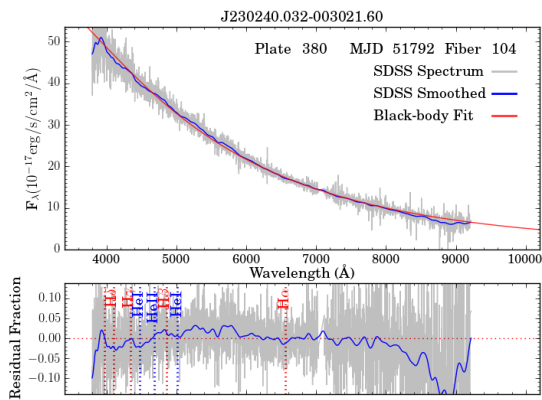
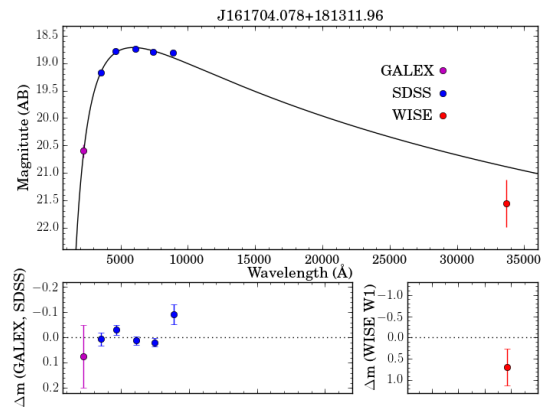
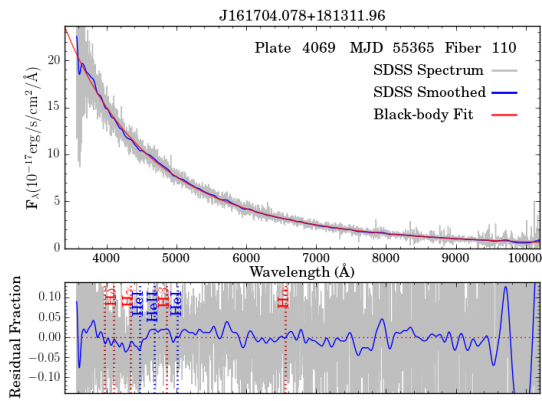
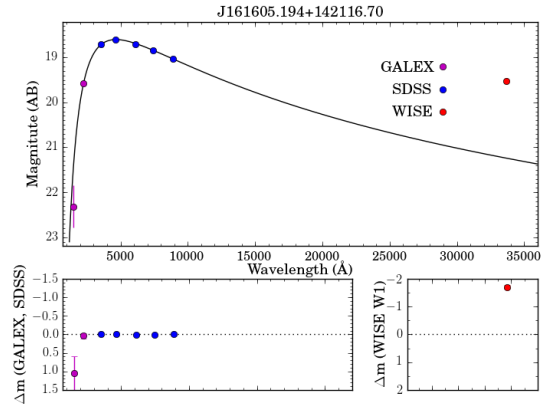
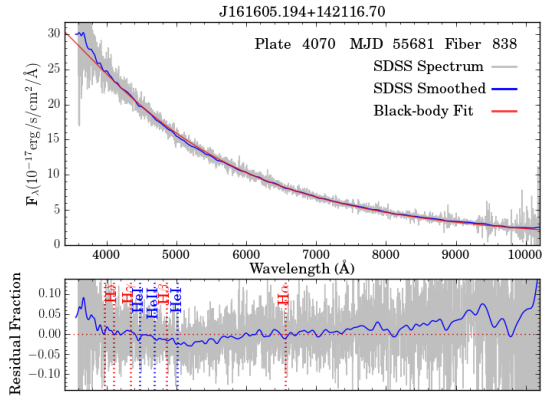












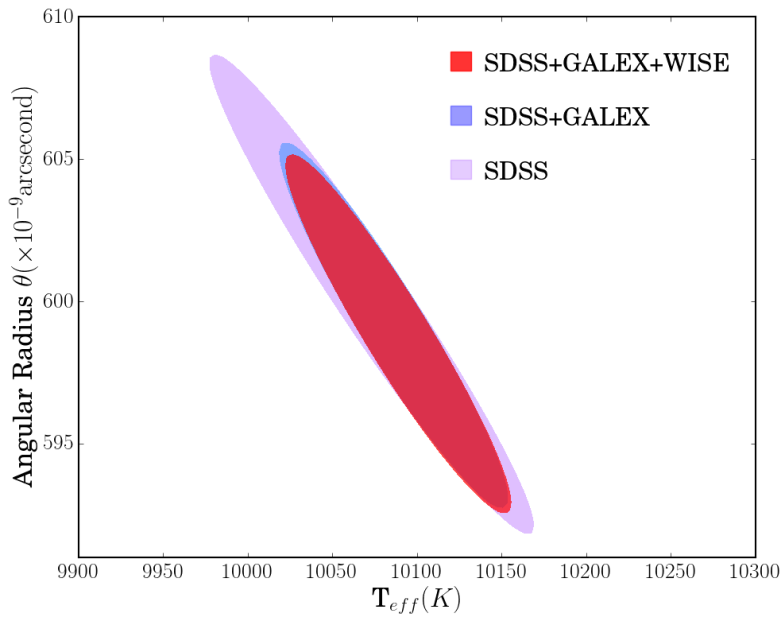


Fig. 2.— Examples of the black-body fit, the fit for J124535.626+423824.58. One sigma outer contour (thin coloured) is the fit to SDSS five-colour photometric data alone and inner contour (thicker coloured) is the fit GALEX UV data included. Inclusion of WISE IR data does not change the contour.

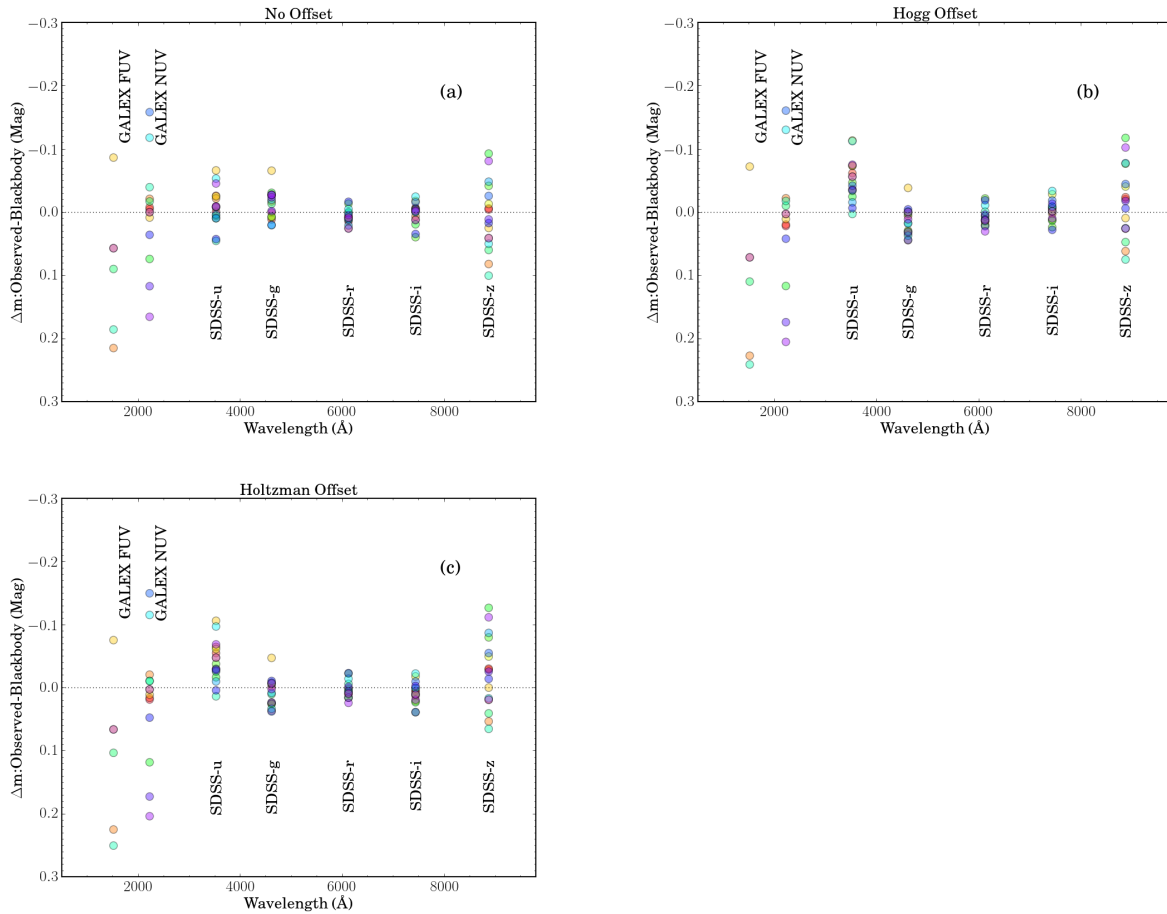


Fig. 3.— (a) Residuals of the SDSS five-band photometric data and the GALEX data from the black body fits in magnitude. (b) The SDSS photometric data are corrected for the offset proposed by Hogg and re-fitting is made to give the best fit. The figure shows residuals in magnitude. (c) The offset is applied to SDSS photometry as suggested by Holtzman et al. (2009) based on the CALSPEC zero point. Another re-fitting is made to give the best black-body fits. The figure shows residuals in magnitude.